The combination of novel airlift magnetic separation loop system and an efficient biosorbent for the removal of Pb(II) from aqueous solution

Xiaolei Li, Huidong Li, Lin Zhang, Kaili Huo, Zhexin Zhang, Jing Li and Hui Xu

ABSTRACT

An efficient biosorbent containing magnetic nanoparticles, walnut shell powder, foam, and alginate (AMWSF) was prepared and used in Pb(II) removal. The adsorption process was performed in an airlift magnetic separation loop system. Optimum adsorption conditions were tested at pH 3–7, biomass dose of 0.03–0.4 g, temperature of 15–35 °C, initial Pb(II) ion concentration of 50–400 mg·L^{-1}, and contact time of 10–480 min. The equilibrium adsorption capacity reached up to 69.45 mg·g^{-1}. The physicochemical properties of AMWSF were analyzed by scanning electron microscopy coupled with energy-dispersive X-ray spectroscopy and Fourier transform infrared spectroscopy. The experimental data were in agreement with the pseudo-second-order kinetic and Langmuir isotherm models. The influences of Cu(II), Cd(II), and Zn(II) on Pb(II) adsorption showed antagonistic effect strength in the order of Cu(II) > Cd(II) > Zn(II). AMWSF was reused seven times and separated rapidly by magnetic field. The results demonstrated the potential of AMWSF in practical applications involving Pb(II).

Key words | airlift loop system, biosorbent, combination, magnetic separation, Pb(II) removal

Xiaolei Li
Huidong Li (corresponding author)
Lin Zhang
Kaili Huo
Zhexin Zhang
Jing Li
Hui Xu
School of Civil Engineering,
Inner Mongolia University of Technology,
Hohhot 010051,
China
E-mail: *lihuidong@imut.edu.cn*

INTRODUCTION

In recent years, with the fast-growing industrial activities, large numbers of heavy metals have been used in different manufacturing activities. Toxic metal ions have been discharged into aquatic ecosystems due to improper disposal. Heavy metals are non-biodegradable and accumulate in the food chain, so they present serious threats to ecosystems and human health. Therefore, it is necessary to remove heavy metal ions or transform them to less toxic forms in water bodies, in order to promote sustainable development. Pb(II) is an indispensable micronutrient to humans, but excessive Pb(II) would disrupt their metabolism and cause several diseases such as digestive disorder, autoimmune disorder, and liver, kidney, stomach and lung cancer (Gola *et al.* 2016). Therefore, heavy metal contamination in industrial wastewater is a global concern at present.

To date, many technologies have been used to decontaminate heavy metal ions from wastewaters, such as chemical precipitation, electrolysis, ion exchange, oxidation reduction, biological treatment, reverse osmosis and membrane filtration (Akram *et al.* 2017; Xu *et al.* 2017a; Shi *et al.* 2018). However, these methods have many disadvantages such as high cost, process complexity and secondary pollution (Yilmaz *et al.* 2011). These drawbacks have made the research focus on an effective technique for heavy metal ions removal. Biosorption has attracted considerable interest in the recent years because of important advantages such as high efficiency, low cost, ease of availability and environmental friendliness (Esmaeili & Khoshnevisan 2016; Safinejad *et al.* 2017). It has been found to be an appropriate choice and suitable for protection of the environment and human health. Various biosorbents have been applied to validate the removal performance of Pb(II). Still, these biosorbents have some defects such as difficult recycling and poor regeneration performance, preventing them from achieving a good status. To solve this issue, developing a biosorbent with excellent regeneration performance is necessary for Pb(II) removal.

Abundant and cheap walnut shell (WS) is often preferentially used in Pb(II) removal. This natural biomaterial contains lignin, cellulose, and hemicellulose, and its

doi: 10.2166/wst.2018.495

structure has various functional groups (Zhu *et al.* 2016). The efficiency of Pb(II) removal increases when WS is used in powdered form. In this work, a good biosorbent (referred to as AMWSF) was prepared by using alginate-coated magnetic nanoparticles, WS powder, and foam. Magnetic nanoparticles were used for rapid separation. In previous studies, biosorption was mainly used for the removal of a single heavy metal, but the water body is a complex system where several heavy metals often coexist in wastewater (Li *et al.* 2017). In Pb(II) removal, other heavy metals influence the process involved.

During adsorption, mechanical stirring may cause serious damage to an adsorbent owing to shear force and may thus affect solid–liquid separation and adsorbent recycling. For this reason, an airlift magnetic separation loop system was designed and an efficient and floating biosorbent was used for Pb(II) removal, as shown in Figure 1.

The aims of the study were as follows: (1) optimize adsorption conditions by investigating the influences of pH, temperature, contact time, biomass dose, and varying Pb(II) concentrations; (2) consider the adsorption mechanism according to the kinetics, isotherm models, and various analysis techniques; (3) investigate the effects of Cu(II), Cd(II), and Zn(II) on Pb(II) adsorption in a binary system; and (4) research the reusability performance of AMWSF through desorption experiments.

EXPERIMENTAL

Materials

The WS was collected from plant residues. Sodium alginate and calcium chloride were supplied by West Long Chemical Co., Ltd (Guangdong, China). Lead nitrate and other chemical agents were all procured from HuaLan Chemical Technology Co., Ltd (Shandong, China). Different concentrations of Pb(II) solutions were prepared from the stock solution of 0.1 mol·L^{-1} by dissolving 33.121 g of lead nitrate in deionized water until the resulting solution had a volume of 1,000 mL. All the required chemicals used were of analytical grade.

Preparation of magnetic nanoparticles, walnut shell and foam encapsulated in calcium alginate

Dirt from walnut shells was removed through repeated washing with deionized water. Then, the shells were dried in an oven at 80 °C for 12 h before they were ground in a ball grinder. The resulting powder particles with diameters of less than 0.6 mm were stored in a zip-top bag. Magnetic nanoparticles (n-Fe_3O_4) were prepared by the co-precipitation method (Mahmoud *et al.* 2016). In this procedure, 8.08 g of $Fe(NO_3)_3{\cdot}9H_2O$ and 2.78 g of $FeSO_4{\cdot}7H_2O$ were

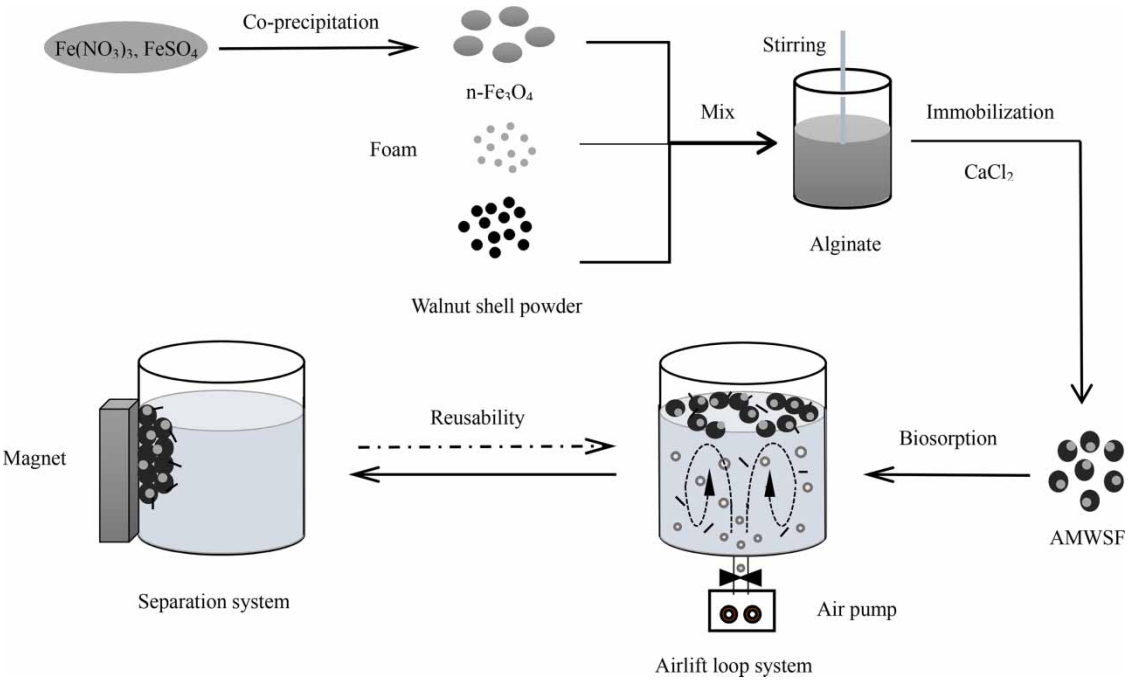

Figure 1 | Schematic route for preparation of AMWSF and airlift magnetic separation loop system.

dissolved in 25 mL of 0.5 M HCl. The mixture was then placed into a three-necked flask, which contained 250 mL of 1.5 M NaOH, with magnetic stirring (400 rpm) for 30 min at 80 °C. The obtained n-Fe_3O_4 particles were separated in the presence of a magnetic field, washed three times with deionized water, and finally dried at 60 °C until complete dryness. The particles were finally placed in a zip-top bag for later use. For AMWSF preparation, 2.5 g of sodium alginate was added to 100 mL of deionized water at 80 °C. The mixture was continuously stirred until the components were completely mixed. Five grams of powder was poured into the beaker and stirred for 30 min. Then, 1.0 g of n-Fe_3O_4 particles was mixed with the above mixture. The final mixture was stirred for another 30 min. The product was dropped into a 3% $CaCl_2$ solution until AMWSF was obtained. AMWSF, which was separated from the $CaCl_2$ solution after 24 h hardening, was rinsed three times with deionized water. The typical size of the AMWSF was about 5.0 mm in diameter. AMWSF was evaluated as Pb(II) adsorbent. As represented in Figure 1, an efficient biosorbent (AMWSF) was obtained, which can be used in Pb(II) removal.

Characterization of AMWSF

Before and after biosorption, the physical and chemical properties of AMWSF were characterized. Surface morphological structure and elemental analysis were conducted with a scanning electron microscope (SEM, Tokyo, Japan) coupled with an energy-dispersive X-ray spectrometer (EDX, Abingdon, Oxfordshire, UK). Fourier transform infrared (FTIR) spectra were obtained, to identify the functional groups on the tested AMWSF, in a PerkinElmer spectrometer using a KBr beam splitter with 4,000–400 cm^{-1} wavenumber and 4 cm^{-1} resolution.

Batch adsorption experiments

The experiments of Pb(II) adsorption on the prepared AMWSF were conducted to study the effects of adsorption parameters, such as pH (3–7), temperature (15–35 °C), biomass dose (0.03–0.4 g), contact time (10–480 min), and Pb(II) concentration (50–400 $mg{\cdot}L^{-1}$). At room temperature, the experiments were performed in 100 mL solutions in a 250 mL reactor. Uniform bubbles flowed into the aqueous solution from the bottom of the reactor. During the initial analyses, 100 mL of solutions with 100 $mg{\cdot}L^{-1}$ of Pb(II) and 0.1 g AMWSF, pH of 5.0, and contact time of 480 min was treated. Suspension pH was adjusted by using 0.1 M HCl and NaOH. The concentration of Pb(II) was determined by flame atomic absorption spectrometry (FAAS).

The adsorption amount could be calculated using equation:

$$q_e = \frac{(C_0 - C_e) \times V}{M} \tag{1}$$

where C_0 and C_e ($mg{\cdot}L^{-1}$) are the initial and equilibrium concentration, respectively; q_e ($mg{\cdot}g^{-1}$) represents the adsorption capacity; V (L) is the volume of solution and M (g) is the biomass dose (dry weight).

Kinetic and isotherm models

The adsorption curves were interpreted by fitting the pseudo-first-order and pseudo-second-order. These equations were described as follows:

$$\ln(q_e - q_t) = \ln(q_e) + k_1 \cdot t \tag{2}$$

$$t/q_t = 1/(k_2 \cdot q_e^2) + t/q_e \tag{3}$$

where k_1 (min^{-1}) and k_2 ($g{\cdot}mg{\cdot}min^{-1}$) are the rate constant of pseudo-first-order and pseudo-second-order, respectively; q_e and q_t ($mg{\cdot}g^{-1}$) are the amount of Pb(II) on AMWSF at equilibrium and at time t (min), respectively.

The adsorption mechanism was studied by applying the Langmuir and Freundlich isotherm models. The linearized equations were as follows:

$$\ln(q_e) = \ln(K_F) + (1/n) \cdot \ln(q_e) \tag{4}$$

$$C_e/q_e = 1/(K_L \cdot q_m) + C_e/q_m \tag{5}$$

where C_e ($mg{\cdot}L^{-1}$) and q_e ($mg{\cdot}g^{-1}$) represent equilibrium Pb(II) concentration and equilibrium adsorption capacity, respectively; q_m ($mg{\cdot}g^{-1}$) is the maximum adsorption capacity; K_L ($L{\cdot}mg^{-1}$) and K_F ($mg{\cdot}g^{-1}$) are the Langmuir and Freundlich adsorption equilibrium constants, respectively.

Effects of co-existing heavy metals ions

Heavy metals (Cu(II), Cd(II), and Zn(II)) were selected in this experiment because they are often detected in industrial wastewater. The competitive effects of Cu(II), Cd(II), and Zn(II) on Pb(II) adsorption were investigated through binary adsorption experiments. Nitrate salts ($Cd(NO_3)_2$, $Cu(NO_3)_2$ and $Zn(NO_3)_2$) were used for the preparation of

these metal solutions. The experiments were carried out at a constant Pb(II) concentration of 100 mg·L^{-1}. Meanwhile, the concentration of co-existing heavy metal ions was 50, 100, 150, and 200 mg·L^{-1}. The solution pH was controlled by 0.1 M NaOH and HCl. All the experiments were set up with three parallel groups, and the average was calculated.

Desorption study

HNO_3 solution (1.0 M) was used as the desorbent for the Pb(II) desorption experiments. AMWSF with adsorbed Pb(II) was rinsed with deionized water for the removal of residual Pb(II) and then added into the HNO_3 solution. The process was allowed to proceed in a 250 mL beaker under the following conditions: 0.1 g·L^{-1} biomass dose, pH 6, 25 °C, and 30 min. Finally, the supernatant was collected for the estimation of Pb(II) by FAAS. The obtained AMWSF was washed three times with deionized water for the subsequent adsorption, which was performed for checking the reusability of AMWSF. The adsorption process was performed for seven cycles.

RESULTS AND DISCUSSION

Characterization of AMWSF

The surface morphology of AMWSF was investigated with a SEM and is illustrated in Figure 2(a) and 2(b). After adsorption (Figure 2(b)), the AMWSF had a rough surface, and massive precipitation was observed in the section. The precipitates might be the deposited Pb(II). Figure 2(c) and 2(d) show the EDX analysis results for the AMWSF. The observed characteristic peak of Pb(II) after adsorption

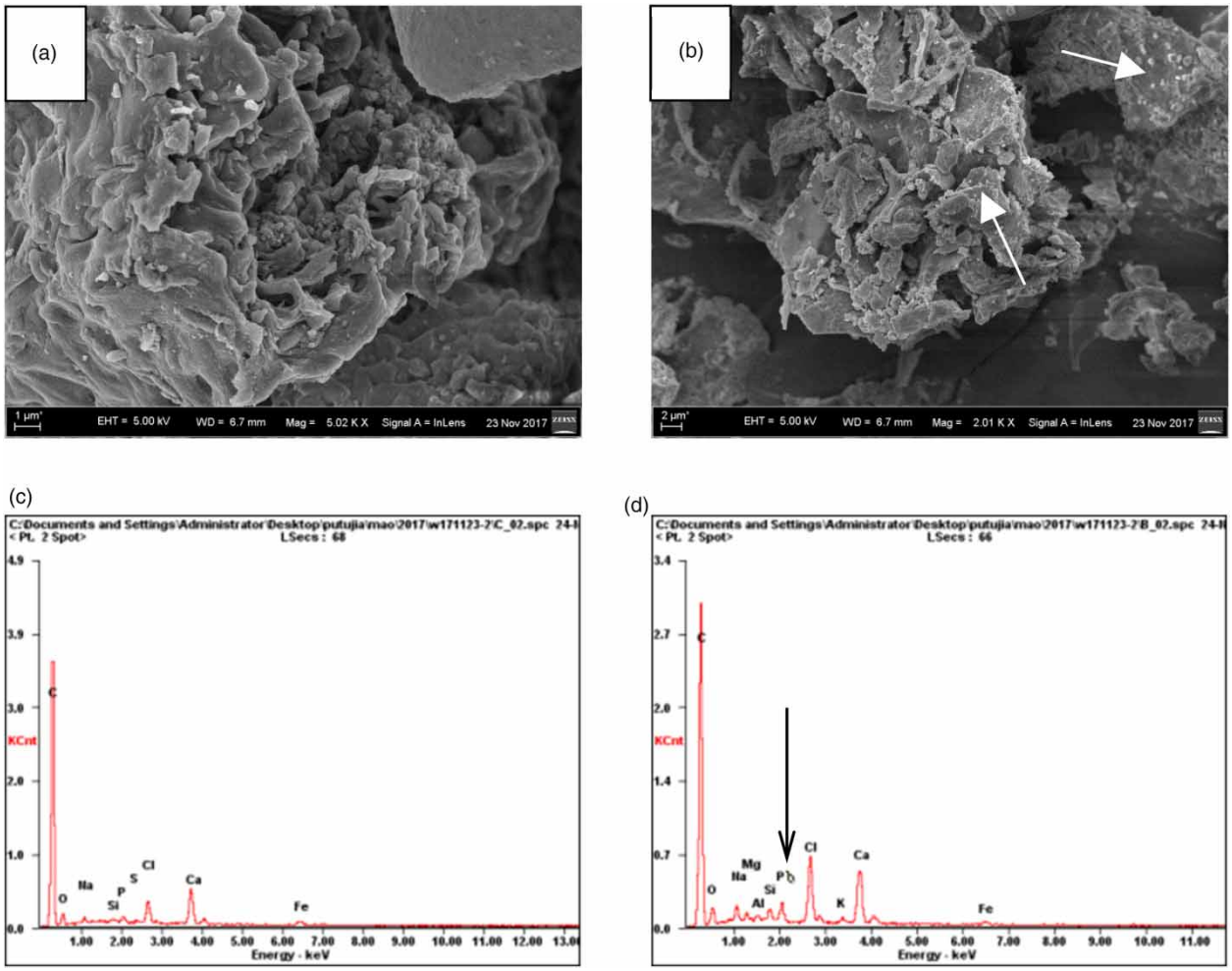

Figure 2 | SEM graphs of AMWSF: (a) before and (b) after adsorption; EDX spectra of AMWSF: (c) control and (d) Pb(II) treated.

Table 1 | Quantitative EDX analysis results before and after adsorption

	Mass (%)	
Element	**Before**	**After**
C	45.52	35.31
O	26.11	30.64
Fe	9.56	9.56
Pb	0	14.21
Others	18.81	10.28

implied that Pb(II) was successfully adsorbed on the AMWSF. Pb(II) content increased by 14.21% after adsorption (Table 1). Finally, the EDX measurements confirmed the formation of Pb(II) precipitate on the AMWSF.

For investigation of the removal mechanism, functional groups interacting with Pb(II) were determined by FTIR. The FTIR spectra obtained from AMWSF before and after adsorption were compared (solid and dashed lines, respectively; Figure 3). No peak appeared or disappeared, but the position of the peaks shifted. The bands at 3,422 cm^{-1} shifted to 3,414 cm^{-1}, implying that –CO and $–NH_2$ participate in Pb(II) adsorption. Another two changes observed from 1,624 cm^{-1} to 1,598 cm^{-1} and from 1,417 cm^{-1} to 1,420 cm^{-1} represented the amide I band stretching and –COO vibration, respectively, and indicated the binding of Pb(II) with the functional groups in the AMWSF surface. In addition, Fe-O appeared at 583 cm^{-1}, confirming the binding of Fe_3O_4 nanoparticles into the AMWSF. The above observations demonstrated that carboxylic, carbonyl, hydroxyl, and amino groups participate in adsorption.

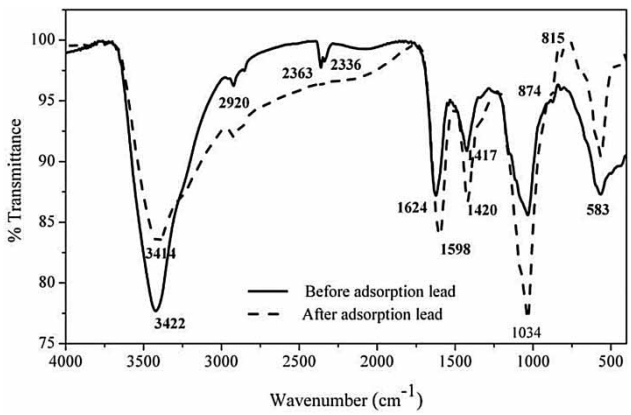

Figure 3 | FTIR spectra of AMWSF in the absence and presence of Pb(II).

Effects of environmental factors on Pb(II) adsorption

The performance of AMWSF for Pb(II) removal was mainly affected by pH, biomass dose, temperature, and initial Pb(II) concentration. Hence, maximum adsorption capacity was obtained through several experiments, which were described earlier in the paper.

To prevent precipitation, the experiments were performed at pH $\leq$7. As shown in Figure 4(a), the adsorption capacity of Pb(II) increased with increasing of pH, and the maximum adsorption ability was 71.87 $mg{\cdot}g^{-1}$. At an extremely acidic pH, the number of H^+ ions competing with Pb^{2+} ions increased in the adsorption active sites. At high pH values, the dissociation of protons occurs from the binding sites, and the amount of Pb^{2+} available for adsorption increased (Tiwari *et al.* 2017). Moreover, some Pb^{2+} ions translated to $Pb(OH)_2$ at pH > 6 and impeded the combination between the other Pb^{2+} ions and surfaces of the functional groups of the biosorbents. Therefore, pH 6 was selected for subsequent adsorption experiments.

The amount of AMWSF dose was varied from 0.03 $g{\cdot}L^{-1}$ to 0.4 $g{\cdot}L^{-1}$. As shown in Figure 4(b), the removal efficiency of Pb(II) increased at increased AMWSF dose, whereas the adsorption capacity was reduced. The low adsorption at a high dose may be due to the constant initial Pb(II) concentration, which was insufficient to completely cover the available active sites on the AMWSF (Masoumi *et al.* 2016). To summarize, an AMWSF dose of 0.1 $g{\cdot}L^{-1}$ was the point at which high removal efficiency was observed and was thus selected for the next experiments.

The effect of temperature on Pb(II) adsorption was studied. As shown in Figure 4(c), the temperature of the adsorption was less significant because the biosorption conformed to energy-independent mechanisms (Ozdemir *et al.* 2009). This result is consistent with those of some studies on Pb(II) biosorption (Masoudzadeh *et al.* 2011; Khadivinia *et al.* 2014). The adsorption experiments were performed at room temperature.

The effect of initial Pb(II) concentration, which ranged from 50 $mg{\cdot}L^{-1}$ to 400 $mg{\cdot}L^{-1}$, was studied. As shown in Figure 4(d), the adsorption capacity of Pb(II) increased at concentrations of up to 300 $mg{\cdot}L^{-1}$ and stabilized thereafter. The high influent metal concentration provided a large driving force for overcoming the entire mass transfer resistance between the aqueous solution and biosorbent (Yu *et al.* 2017). Meanwhile, adsorption stability can be attributed to the lack of binding sites for complexation at high Pb(II) concentrations.

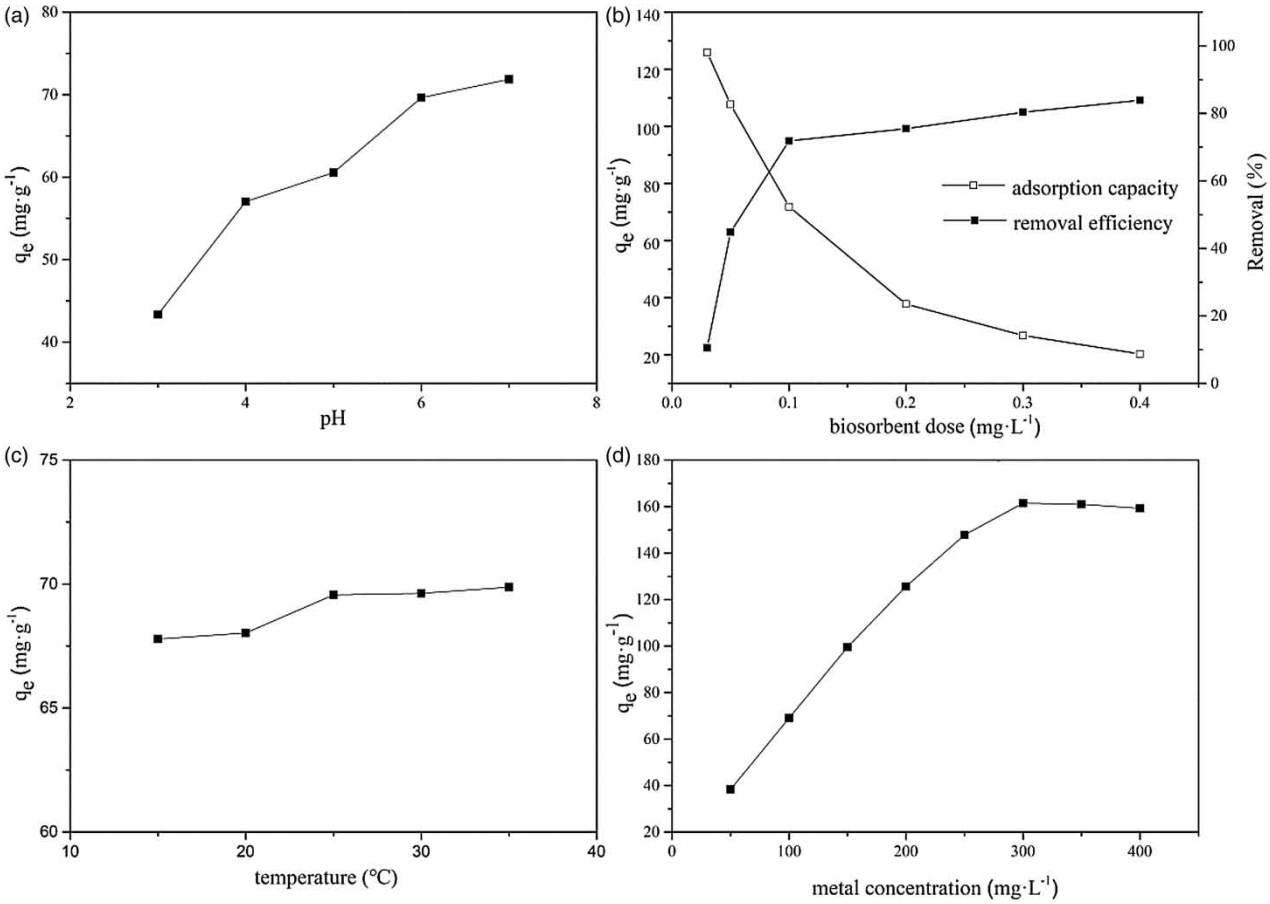

Figure 4 | Effect of pH (a), biomass dose (b), temperature (c), and Pb(II) concentration (d) on the biosorption of Pb(II).

Adsorption kinetics

To predict the rate for Pb(II) removal and interpret the kinetic mechanism of adsorption process, the effect of contact time on the removal efficiency of Pb(II) was studied. The adsorption capacity increased sharply within 60 min and then slowly until it reached equilibrium at 180 min (Figure S1, available with the online version of this paper). Therefore, 180 min was selected as the optimum contact time in this study. The initial fast adsorption was attributed to sufficient unutilized activated sites and low mass transfer resistance (Wang *et al.* 2017). In the subsequent step, the adsorption process was slowed possibly because of the decrease in available binding sites, and thus the Pb(II) adsorption capacity remained constant.

The pseudo-first- and pseudo-second-order kinetic models were employed to fit with the experimental data. The obtained correlation coefficient (R^2) was used for assessing the applicability of each model. The model with the higher R^2 value was considered a more suitable model (Islam *et al.* 2017). The calculated results of kinetic parameter (Figure S2 and Table 2; Figure S2 is available with the online version of this paper) suggested that the Pb(II) data can be simulated better by the pseudo-second-order kinetic model (0.9996) than by the pseudo-first-order kinetic model (0.9641). Moreover, the calculated constants generated by the pseudo-second-order kinetic model were close to the experimental data, implying that Pb(II) adsorption was strongly dependent on available activated sites, and the pseudo-second-order kinetic mechanism was dependent on the concentrations and nature of the adsorbate and adsorbents (Tiwari *et al.* 2017).

Adsorption isotherm

To elucidate the Pb(II) adsorption mechanism, adsorption behavior was studied by two experimental adsorption isotherms. The Langmuir and Freundlich models were utilized to fit the experimental data and reflect adsorption type. The Langmuir model was applied for explaining homogeneous adsorption systems involving monolayer adsorption where no interaction among sorbed molecules occur. The

Table 2 | Model results of AMWSF adsorption kinetics data

	Pseudo-first-order			Pseudo-second-order		
$q_{e,exp}$ (mg·g^{-1})	k_1 (min^{-1})	$q_{e,1}$ (mg·g^{-1})	R^2	k_2 (g·mg^{-1}·min^{-1})	$q_{e,2}$ (mg·g^{-1})	R^2
69.45	0.0096	32.47	0.9641	0.0011	71.74	0.9996

Freundlich equation was proposed as an empirical equation for multilayer heterogeneous adsorption (Benettayeb *et al.* 2017; Zhang *et al.* 2017).

The corresponding results are summarized in Figure S3 and Table 3 (Figure S3 is available with the online version of this paper). The R^2 value obtained from the Langmuir isotherm (0.9874) was higher than that of the Freundlich isotherm (0.7752), indicating that the adsorption behavior followed the Langmuir model equation. Moreover, the theoretical maximum adsorption values from the Langmuir equation were all 170.36 mg·g^{-1} for Pb(II), which was close to the experimental value (160.45 mg·g^{-1}). The effect of the isotherm shape can be expressed in terms of the equilibrium parameter R_L, also known as the separation factor, which can be used to predict whether an adsorption system is unfavorable or favorable. R_L can be calculated as $1/(1 + K_L \cdot C_0)$. If $R_L = 0$, adsorption is irreversible; if $0 < R_L < 1$, it is favorable; if $R_L = 1$, it is linear; and adsorption is unfavorable if $R_L > 1$. In this study, R_L value was 0.9423 for the initial Pb(II) concentration of 100 mg·L^{-1}, suggesting that the adsorption process was favorable. In summary, the results showed that monolayer adsorption of the active sites on the AMWSF surface played a major role in Pb(II) removal.

Effects of co-existing heavy metals ions

In general, industrial effluents are multi-metal ion systems. Other metal ions interfere with the adsorption of target metal ions (Jones *et al.* 2016; Wang *et al.* 2016). Compared with common metal ions, heavy metal ions considerably affect adsorption. Several studies reported that the effects are mostly synergetic, antagonistic, and with no interaction. Thus, determining the effects of Cu(II), Cd(II), and Zn(II) on Pb(II) adsorption by AMWSF is necessary. In the present study, the effects of competing ions were studied by using a binary system (Cu/Pb, Cd/Pb and Zn/Pb). As plotted in Figure 5, the adsorption capacity of Pb(II) showed a downward trend in binary systems with increased Cu(II), Cd(II) and Zn(II) concentrations. The increase was attributed to the heavy metal ions that competed with Pb(II) for available sites on the AMWSF. The results indicated that these ions had an inhibiting effect on Pb(II) adsorption, and this effect was intensified when the concentrations of the competing ions increased. The difference between the Pb(II) adsorption capacities of the binary systems was attributed to the different physicochemical characteristics of heavy metal ions (Wang *et al.* 2017). Some studies suggested that electronegativity plays a vital role in metal adsorption processes. Heavy metals have different ionic radii, indicating that their electronegativity varies. The electronegativity values were 2.33, 1.90, 1.69 and 1.65 for Pb(II), Cu(II), Cd(II) and Zn(II), respectively. The higher electronegativity of heavy metals meant they were more easily attracted by adsorbents (Wang *et al.* 2018). Thus Pb(II) had a larger covalent index and exhibited a higher affinity than Cu(II), Cd(II) and Zn(II), which was also the reason why the adsorption capacity of Pb(II) showed no significant decline in this study.

Desorption study

For practical application, biosorbent reuse is extremely important because this procedure reduces processing cost (Xu *et al.* 2017b). To investigate the reusability of AMWSF, the desorption experiments were repeated for seven cycles. In this study, HNO_3 solution (1.0 M) was used for the desorption of Pb(II). Then, AMWSF was rinsed with deionized water for reuse in the next cycle. Finally, AMWSF was rapidly separated from the liquid phase by using an external magnetic field. From Figure 6, the adsorption capacity of AMWSF had a decreasing trend with increasing reuse, and

Table 3 | Langmuir and Freundlich isotherm parameters for adsorption of Pb(II) on AMWSF

	Langmuir			Freundlich		
$q_{m,exp}$ (mg·g^{-1})	q_m (mg·g^{-1})	K_L (L·mg^{-1})	R^2	K_F (mg·g^{-1})	n	R^2
160.45	170.36	0.9423	0.9874	42.476	3.9261	0.7752

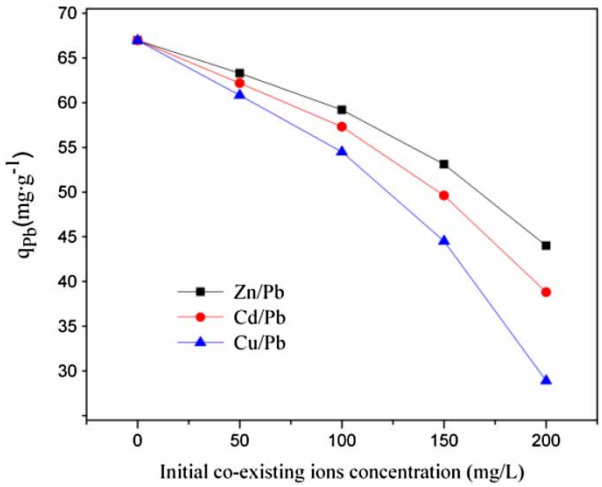

Figure 5 | Effect of Cu, Cd, and Zn(II) concentration on the Pb(II) adsorption.

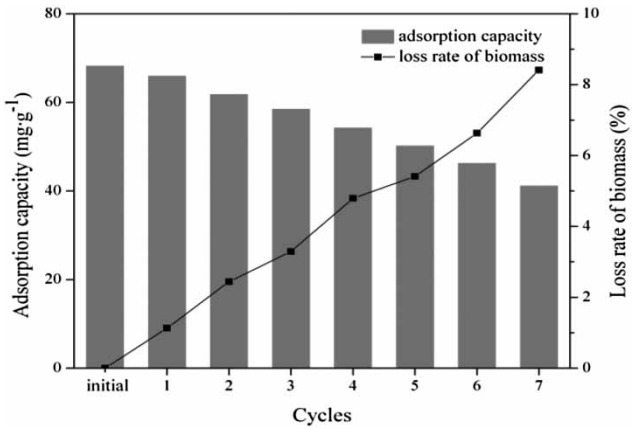

Figure 6 | Adsorption capacity and loss rate of biomass after seven repeated cycles for Pb(II) biosorption on AMWSF.

the decline was ascribed to the activated binding sites occupied by Pb(II) having not released completely. However, no significant decline was observed, and the airlift loop system reduced the mass loss of AMWSF. Furthermore, the adsorption capacity of AMWSF when used for one and seven times were 65.93 and 41.12 mg·g^{-1}, respectively. Meanwhile, the loss rate of AMWSF decreased by 8.41% after seven consecutive cycles. Finally, AMWSF is suitable for cyclic utilization for Pb(II) removal and this good performance implied its high potential application.

CONCLUSIONS

In this study, the optimization of pH, biomass dose, temperature, initial concentration, and contact time was achieved at 6, 0.1 g, 25 °C, and 180 min, respectively. The equilibrium adsorption capacity of up to 69.45 mg·g^{-1} was achieved, and the adsorption process can be described well by the pseudo-second-order kinetic and Langmuir isotherm models. The adsorption mechanism demonstrated that the deposition of Pb(II) was due to the functional carboxylic, hydroxyl, carbonyl and amino groups. Co-existing heavy metals (Cu(II), Cd(II) and Zn(II)) have an antagonistic effect during Pb(II) removal, and AMWSF can be efficiently reused up to seven times because of the airlift magnetic separation loop system that does not cause shear force damage to AMWSF. Overall, AMWSF was found to be an efficient adsorbent for Pb(II) removal in an airlift magnetic separation loop system.

ACKNOWLEDGEMENTS

This work was supported by the Natural Science Foundation of Inner Mongolia Autonomous Region (2017MS0217) and Science Research Program of Higher Education Institutions of Inner Mongolia Autonomous Region (NJZY16084).

REFERENCES

Akram, M., Bhatti, H. N., Iqbal, M., Noreen, S. & Sadaf, S. 2017 Biocomposite efficiency for Cr(VI) adsorption: kinetic, equilibrium and thermodynamics studies. *Journal of Environmental Chemical Engineering* **5**, 400–411.

Benettayeb, A., Guibal, E., Morsli, A. & Kessas, R. 2017 Chemical modification of alginate for enhanced sorption of Cd(II), Cu(II) and Pb(II). *Chemical Engineering Journal* **316**, 704–714.

Esmaeili, A. & Khoshnevisan, N. 2016 Optimization of process parameters for removal of heavy metals by biomass of Cu and Co-doped alginate-coated chitosan nanoparticles. *Bioresource Technology* **218**, 650–658.

Gola, D., Dey, P., Bhattacharya, A., Mishra, A., Malik, A., Namburath, M. & Ahammad, S. Z. 2016 Multiple heavy metal removal using an entomopathogenic fungi *Beauveria bassiana*. *Bioresource Technology* **218**, 388–396.

Islam, M. S., Choi, W. S., Nam, B., Yoon, C. & Lee, H. J. 2017 Needle-like iron oxide@$CaCO_3$ adsorbents for ultrafast removal of anionic and cationic heavy metal ions. *Chemical Engineering Journal* **307**, 208–219.

Jones, B. O., John, O. O., Luke, C., Ochieng, A. & Bassey, B. J. 2016 Application of mucilage from *Dicerocaryum eriocarpum* plant as biosorption medium in the removal of selected heavy metal ions. *Journal of Environmental Management* **177**, 365–372.

Khadivinia, E., Sharafi, H., Hadi, F., Zahiri, H. S., Modiri, S., Tohidi, A., Mousavi, A., Salmanian, A. H. & Noghabi, K. A. 2014 Cadmium biosorption by a glyphosate-degrading

bacterium, a novel biosorbent isolated from pesticide-contaminated agricultural soils. *Journal of Industrial and Engineering Chemistry* **20**, 4304–4310.

Li, M. F., Liu, Y. G., Liu, S. B., Shu, D., Zeng, G. M., Hu, X. J., Tan, X. F., Jiang, L. H., Yan, Z. L. & Cai, X. X. 2017 Cu(II)-influenced adsorption of ciprofloxacin from aqueous solutions by magnetic graphene oxide/nitrilotriacetic acid nanocomposite: competition and enhancement mechanisms. *Chemical Engineering Journal* **319**, 219–228.

Mahmoud, M. E., Abdou, A. E. H., Mohamed, S. M. S. & Osman, M. M. 2016 Engineered *Staphylococcus aureus* via immobilization on magnetic Fe_3O_4-phthalate nanoparticles for biosorption of divalent ions from aqueous solutions. *Journal of Environmental Chemical Engineering* **4**, 3810–3824.

Masoudzadeh, N., Zakeri, F., Lotfabad, T. B., Sharafi, H., Masoomi, F., Zahiri, S. H., Ahmadian, G. & Noghabi, K. A. 2011 Biosorption of cadmium by *Bervendimonas* sp. ZF12 strain, a novel biosorbent isolated from hot-spring waters in high background radiation areas. *Journal of Hazardous Materials* **197**, 190–197.

Masoumi, F., Khadivinia, E., Alidoust, L., Mansourinejad, Z., Shahryari, S., Safaei, M., Mousavi, A., Salmanian, A. H., Zahiri, H. S., Vali, H. & Noghabi, K. A. 2016 Nickel and lead biosorption by *Curtobacterium* sp. FM01, an indigenous bacterium isolated from farmland soils of northeast Iran. *Journal of Environmental Chemical Engineering* **4**, 950–957.

Ozdemir, S., Kilinc, E., Poli, A., Nicolaus, B. & Guven, K. 2009 Biosorption of Cd, Cu, Ni, Mn and Zn from aqueous solutions by thermophilic bacteria, *Geobacillus toebii* sub. sp. *decanicus* and *Geobacillus thermoleovorans* sub. sp. *stromboliensis*: equilibrium, kinetic and thermodynamic studies. *Chemical Engineering Journal* **152**, 195–205.

Safinejad, A., Chamjangali, M. A., Goudarzi, N. & Bagherian, G. 2017 Synthesis and characterization of a new magnetic bio-adsorbent using walnut shell powder and its application in ultrasonic assisted removal of lead. *Journal of Environmental Chemical Engineering* **5**, 1429–1437.

Shi, J. H., Yang, Z. X., Dai, H. L., Lu, X. W., Peng, L. H., Tan, X. Y., Shi, L. J. & Fahim, R. 2018 Preparation and application of modified zeolites as adsorbents in wastewater treatment. *Water Science & Technology*. doi: 10.2166/wst.2018.249.

Tiwari, S., Hasan, A. & Pandey, L. M. 2017 A novel bio-sorbent comprising encapsulated *Agrobacterium fabrum* (SLAJ731) and iron oxide nanoparticles for removal of crude oil co-contaminant, lead Pb(II). *Journal of Environmental Chemical Engineering* **5**, 442–452.

Wang, N. N., Xu, X. J., Li, H. Y., Zhai, J. I., Yuan, L. Z., Zhang, K. X. & Yu, H. W. 2016 Preparation and application of a xanthate-modified thiourea chitosan sponge for the removal of Pb(II) from aqueous solutions. *Industrial & Engineering Chemistry Research* **55**, 4960–4968.

Wang, N. N., Xu, X. J., Li, H. Y., Wang, Q. Y., Yuan, L. Z. & Yu, H. W. 2017 High performance and prospective application of xanthate-modified thiourea chitosan sponge-combined *Pseudomonas putida* and *Talaromyces amestolkiae* biomass for Pb(II) removal from wastewater. *Bioresource Technology* **233**, 58–66.

Wang, Y. Y., Liu, Y. X., Lu, H. H., Yang, R. Q. & Yang, S. M. 2018 Competitive adsorption of Pb(II), Cu(II), and Zn(II) ions onto hydroxyapatite-biochar nanocomposite in aqueous solutions. *Journal of Solid State Chemistry* **261**, 53–61.

Xu, X. J., Li, H. Y., Wang, Q. Y., Li, D. D., Han, X. R. & Yu, H. W. 2017a A facile approach for surface alteration of *Pseudomonas putida* I3 by supplying K_2SO_4 into growth medium: enhanced removal of Pb(II) from aqueous solution. *Bioresource Technology* **232**, 79–86.

Xu, J., Yuvaraja, G. & Zhang, W. J. 2017b Application of chitosan/poly(vinyl alcohol)/CuO (CS/PVA/CuO) beads as an adsorbent material for the removal of Pb(II) from aqueous environment. *Colloid and Surface B: Biointerfaces* **149**, 184–195.

Yilmaz, A. E., Boncukcuoglu, R., Kocakerim, M. & Karakas, I. H. 2011 Waste utilization: the removal of textile dye (Bomaplex Red CR-L) from aqueous solution on sludge waste from electrocoagulation as adsorbent. *Desalination* **277**, 156–163.

Yu, J., Wang, J. L. & Jiang, Y. Z. 2017 Removal of uranium from aqueous solution by alginate beads. *Nuclear Engineering and Technology* **49**, 534–540.

Zhang, S. W., Yang, H. C., Huang, H. Y., Gao, H. H., Wang, X. X., Cao, R. Y., Li, J. X., Xu, X. J. & Wang, X. K. 2017 Unexpected ultrafast and high adsorption capacity of oxygen vacancy-rich WOx/C nanowire networks for aqueous Pb^{2+} and methylene blue removal. *Journal of Materials Chemistry A* **5**, 15913–15922.

Zhu, M., Yao, J., Dong, L. & Sun, J. J. 2016 Adsorption of naphthalene from aqueous solution onto fatty acid modified walnut shells. *Chemosphere* **144**, 1639–1645.

First received 20 June 2018; accepted in revised form 22 November 2018. Available online 6 December 2018